Confused-Prism[5]arene: a Conformationally Adaptive Host by Stereoselective Opening of the 1,4-Bridged Naphthalene Flap

Paolo Della Sala,[a] Rocco del Regno,[a] Amedeo Capobianco,*[a] Veronica Iuliano,[a] Carmen Talotta,[a] Silvano Geremia,*[b] Neal Hickey,[b] Placido Neri,[a] and Carmine Gaeta*[a]

Abstract: The confused-prism[5]arene macrocycle (*c*-**PrS[5]^{Me}**) shows conformational adaptive behavior in the presence of ammonium guests. Upon guest inclusion, the 1,4-bridged naphthalene flap reverses its planar chirality from p*S* to p*R* (with reference to the p*S*(p*R*)$_4$ enantiomer). Stereoselective directional threading is also observed in the presence of directional axles, in which *up/down* stereoisomers of homochiral (p*R*)$_5$-*c*-**PrS[5]^{Me}** pseudorotaxanes are formed.

Introduction

Macrocycles[1] are ubiquitous in supramolecular chemistry. They have found applications in different fields, such as molecular recognition,[2] catalysis,[3] and as building blocks in self-assembled architectures.[4] Taking inspiration from natural receptors, macrocyclic hosts are designed to incorporate a biomimetic internal cavity which can host complementary guests. In addition to the classical macrocycles, such as calixarenes,[5] resorcinarenes[6] and pillararenes,[7] very recently many efforts have been made to synthesize deep-cavity macrocycles[8] based on macrocyclization of naphthol monomers. Among these, naphthotubes,[9] calixnaphtharene,[10] oxatubarene[11] and saucerarenes,[12] show peculiar conformational and structural properties. Aromatic macrocyclic hosts typically exhibit considerable conformational versatility; for example, due to the potential relative orientations of the *n* constitutive phenol rings, each calix[*n*]arene macrocycle can adopt a variety of molecular conformations,[5] which directly influence its supramolecular properties. Macrocycles with high conformational mobility often show adaptive behaviors in the presence of complementary guests.[13] Interestingly, conformational adaptive processes induced by the presence of substrates are widely diffuse in biological systems.[14] Natural processes, such as protein–substrate binding, often involve conformational changes of the protein, which can occur through two limiting mechanisms: prior to the ligand binding event ("conformational selection"[14]) or after the ligand binding event ("induced fit").[15,16] In the conformational-selection binding model, protein conformational changes can occur before the ligand binding, and the binding of the substrate stabilizes a specific conformation of the protein. In induced-fit binding model,[14] the conformational change is induced by the ligand and occurs upon substrate binding.[17]

Recently, the oxatub[4]arene macrocycle reported by Wei Jiang[11] has shown biomimetic conformational adaptive behavior,[13] as it can adopt four conformations interconvertible by flipping of naphthalene rings. The authors showed that, in agreement with the model of the "conformational selection", specific ammonium guests selected the best-fit conformer, thus altering the equilibrium distribution in its favor, at the expense of other conformations. Analogously, we showed that the complexation of secondary ammonium cations selects the cone and partial cone conformations of calix[5]arene.[18] Therefore, also calix[*n*]arenes are capable of exhibiting a conformational response to ammonium guests. In addition, our recently reported calix [2]naphth[2]arene macrocycle[10] which can adopt five possible conformations, shows, in the presence of alkali metal cations, only the 1,2-alternate conformation to achieve the optimal binding.

In 2020, we reported a novel class of macrocycles named prism[*n*]arenes constituted by methylene-bridged 2,6-dialkoxynaphthalene units (Figure 1, top). [19–24] In the symmetric prism[*n*]arene, the naphthol rings are all linked at their 1,5-positions (Figure 1, top left and right). The C–C single bridging bonds on positions 1 and 5 are not aligned, which partially hinders the mutual rotation of the naphthalene moieties. This conformational property is an important aspect of the preorganization of these dissymmetric macrocyclic hosts.[19–24] Methoxy-

[a] *Dr. P. Della Sala, R. del Regno, Prof. A. Capobianco, V. Iuliano, C. Talotta, Prof. P. Neri, Prof. C. Gaeta*
Laboratory of Supramolecular Chemistry
Department of Chemistry and Biology "A. Zambelli"
University of Salerno
Via Giovanni Paolo II,
84084, Fisciano, Salerno (Italy)
E-mail: cgaeta@unisa.it
acapobianco@unisa.it

[b] *Prof. S. Geremia, Prof. N. Hickey*
Centro di Eccellenza in Biocristallografia
Dipartimento di Scienze Chimiche e Farmaceutiche
Università di Trieste
Via L. Giorgieri 1,
34127 Trieste (Italy)
E-mail: sgeremia@units.it

Supporting information for this article is available on the WWW under https://doi.org/10.1002/chem.202203030

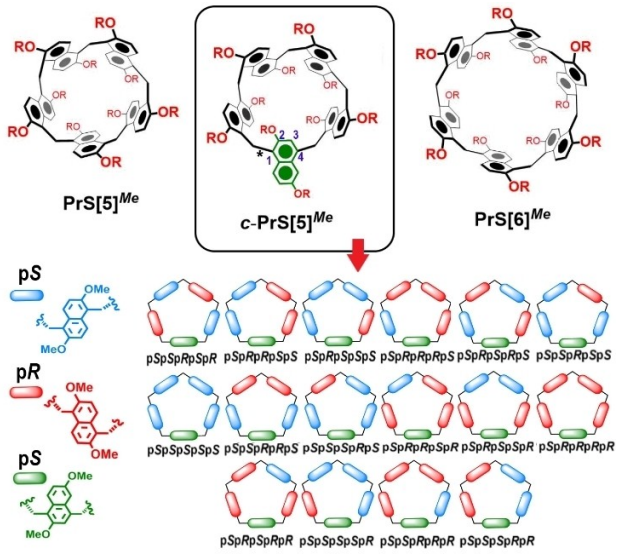

Figure 1. (Top) Chemical drawing of prismarene macrocycles and (bottom) schematic representation of the 16 diastereoisomers (each as an enantiomeric pair) of *c*-**PrS[5]^{Me}** generated by the various configurations of the chiral planes.

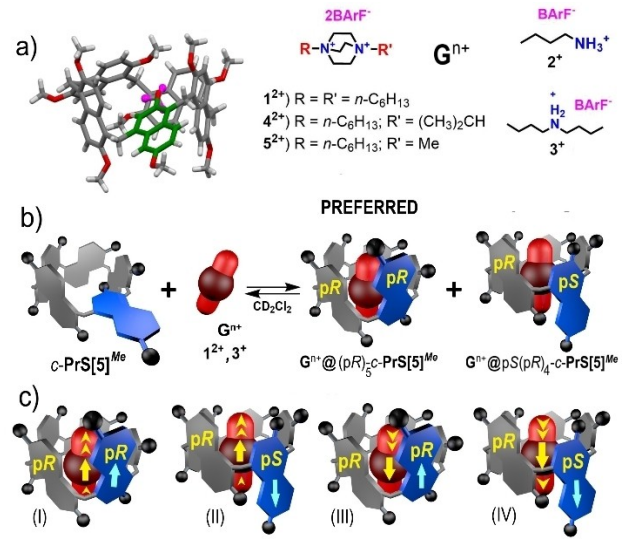

Figure 2. a) The p*S*(p*R*)$_4$-*c*-**PrS[5]Me** lowest-energy conformation as obtained by Monte Carlo simulated annealing and successive DFT optimization. b) Schematic representation of possible **G**$^{n+}$**@*c*-PrS[5]^{Me}** stereoisomeric complexes potentially obtainable by threading/*endo*-cavity complexation of the ***c*-PrS[5]^{Me}** host with ammonium guests **1**–**5**. c) For the assignment of *up* and *down* stereochemistry see ref. [28a]. I) (*U*)-**G**$^{n+}$@(p*R*)$_5$-*c*-**PrS[5]^{Me}**. II) (*D*)-**G**$^{n+}$@p*S*(p*R*)$_4$-*c*-**PrS[5]^{Me}**. III) (*D*)-**G**$^{n+}$@(p*R*)$_5$-*c*-**PrS[5]^{Me}**. IV) (*U*)-**G**$^{n+}$@p*S*(p*R*)$_4$-*c*-**PrS[5]^{Me}**.

prismarenes **PrS[*n*]^{Me}** were obtained by reaction of the 2,6-dimethoxynaphthalene with paraformaldehyde in the presence of TFA and dry 1,2-dichloroethane (1,2-DCE) as solvent at 70 °C. Prism[*n*]arenes show a deep π-electron rich aromatic cavity which exhibits a great affinity for quaternary ammonium guests. The 2,6-dimethoxynaphthalene-based prismarenes **PrS[*n*]^{Me}** were obtained by template effect in a thermodynamically controlled synthesis,[19] in which the pentameric prism[5]arene **PrS[5]^{Me}** (Figure 1, top left) and the hexameric prism[6]arene **PrS[6]^{Me}** (Figure 1, top right) were selectively isolated from the equilibrium mixture by using their complementary guests, respectively, 1,4-dihexyl-DABCO (**1**$^{2+}$) and tetraethylammonium cations (Figure 2a).[19,25] Differently, when the reaction was performed in the absence of an ammonium guest, the 1,4-confused-prism[5]arene *c*-**PrS[5]^{Me}** (Figure 1, top middle, and Figure 2a) was preferentially formed by solvent template effect.[19]

The 1,4-confused-prism[5]arene *c*-**PrS[5]^{Me}** is constituted by 4/5 of the naphthalene rings bridged through their 1,5-positions, while the remaining naphthalene group shows a 1,4-bridging pattern (confused-naphthalene ring in green in Figure 1). In this case, the molecule is asymmetric and the two C–C bridging single bonds on positions 1,4 are aligned in such a way that the corresponding naphthalene moiety can in principle rotate more freely. This structural feature of the *c*-**PrS[5]^{Me}** macrocycle makes it as an ideal candidate to study conformational adaptive processes in the presence of appropriate guests.

Results and Discussion

Prism[*n*]arenes exhibit planar chirality, and analogously to pillararene macrocycles,[26] the chirality of each stereogenic plane can be described with p*R* and p*S* descriptors, here defined by the sign of the C–CH$_2$–C1–C2 torsion angles (pages S23–S26 in the Supporting Information, Figure 1).[27] *c*-**PrS[5]^{Me}** can adopt in principle 32 conformations of different planar chiralities, corresponding to 16 enantiomeric pairs (Figure 1), which can interconvert by rotation of the naphthalene units around the methylene bridges.

In order to investigate the stability of the 16 conformers of *c*-**PrS[5]^{Me}** (Figure 1) an exhaustive computational conformational search was performed (see the Supporting Information). An initial guess of the equilibrium geometry of each structure was obtained by molecular mechanics (MM) computations using the MMFF94 force field. Later, the conformer distribution was obtained by a conformer search based on the Monte Carlo simulated annealing procedure. Finally, DFT geometry optimizations were carried out (Supporting Information).

The structure of the lowest-energy conformer (Figure 2a) shows the 1,4-bridged naphthalene ring inserted in the core of the macrocycle, with a negative C–CH$_2$–C1–C2 torsion angle value of −25° (p*S*, Supporting Information). In this conformation, which shows a pseudo-C_2 symmetry, the 2-OMe group (in magenta in Figure 2a) points inside the cavity to establish C–H···π interactions with the aromatic walls with an average C–H···π^{centroid} distance of 3.1 Å (Supporting Information, Figure 3a). The remaining four naphthalene rings, bridged through their 1,5-positions, adopt the p*R* conformation, (p*R*)$_4$. Thus, the

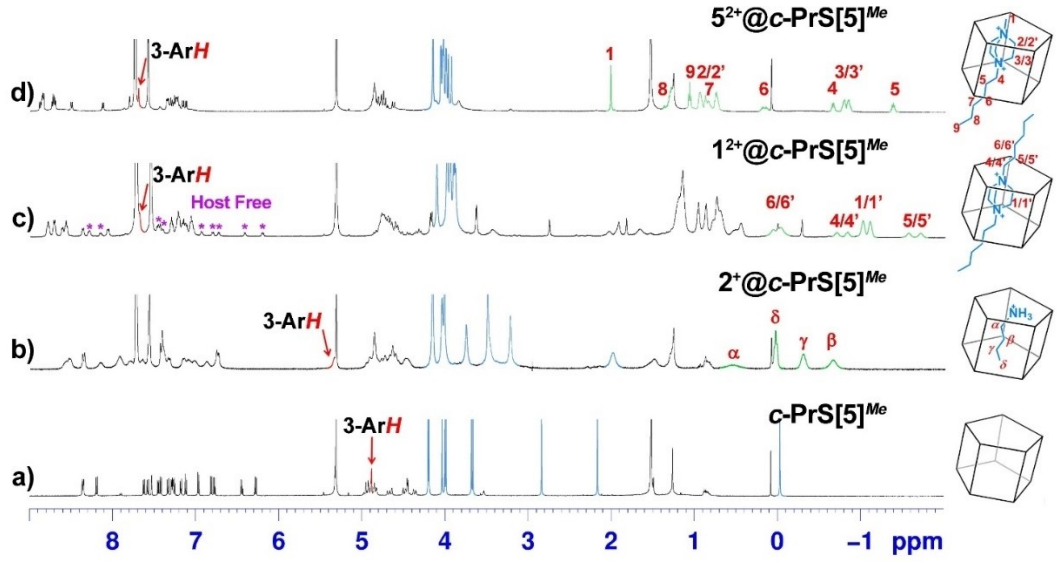

Figure 3. ^{1}H NMR spectra of a) *c*-**PrS[5]^{Me}** in CD_2Cl_2 (600 MHz), b) a 1:1 mixture of *c*-**PrS[5]^{Me}** and **2**$^+$·BArF (4.10 mM) at 298 K, c) a 1:1 mixture of *c*-**PrS[5]^{Me}** and **1**$^{2+}$·$(BArF)_2$ (2.85 mM) at 183 K and d) a 1:1 mixture of *c*-**PrS[5]^{Me}** and **5**$^{2+}$·$(BArF)_2$ (4.10 mM) at 298 K. Guest signals shielded inside the macrocycle are colored in green; red signals (red arrows) indicate the 3-ArH atom of the 1,4-naphthalene ring; the OMe signals of the macrocycle are colored in blue.

p*S*(p*R*)$_4$ conformer (and the enantiomer p*R*(p*S*)$_4$) is found to be far more stable than all other arrangements both by MM and DFT computations. According to DFT results, the second most stable conformer belong to the (p*S*)$_5$ (or (p*R*)$_5$) homochiral family, but it lies + 3.5 kcal mol^{-1} higher than the global minimum (Table S2). Finally, calculations indicate that the other heterochiral conformations of *c*-**PrS[5]^{Me}** are higher in energy by 4–10 kcal mol^{-1} (Supporting Information) than the lowest energy conformation p*S*(p*R*)$_4$ in Figure 2a. Previously,[19] two pseudo-polymorphic forms of *c*-**PrS[5]^{Me}** (α = monoclinic form, β = triclinic form) were reported, which are composed of a racemic mixture of p*R*(p*S*)$_4$ and p*S*(p*R*)$_4$ molecules in the unit cell, which is in agreement with the higher calculated stability for the isolated molecule in this conformation. The strong similarity between the X-ray structure and the predicted minimum energy conformation is confirmed by a rmsd value of 0.20 Å.

Upon complexation with ammonium guests (Figure 2), the stereochemistry of the resulting complexes becomes even more complicated due to the potential formation of directional isomers (up and down in Figure 2c) in the case of directional guests (**2**$^+$, **4**$^{2+}$, **5**$^{2+}$) with respect to the twofold symmetric ones (**1**$^{2+}$, **3**$^+$ in Figure 2b). In the former case, the two possible orientations of the directional guest (*up*/down in Figure 2c)[28a] in the macrocycle doubles the number of possible stereoisomeric complexes with respect to those obtainable with **1**$^{2+}$, **3**$^+$ in Figure 2b.[28] However, if the analysis is restricted to the most stable all-p*R* (or all-p*S*) conformations of the 1,5-naphtalene rings observed for the free host, then the question arises as to whether the 1,4-bridged naphthalene flap (in blue in Figure 2) of *c*-**PrS[5]^{Me}**, which is p*S* (or p*R*) in the free host, opens to adopt a p*R* or p*S* conformation (Figure 2b).

Solid-state structural analysis of the pseudorotaxane **1**$^{2+}$@*c*-**PrS[5]^{Me}** with BArF[29] counterions clearly revealed that the centrosymmetric triclinic crystals are composed of a racemic mixture of homochiral (p*S*)$_5$ and (p*R*)$_5$ conformations (Figure 4a). The central bicyclic unit of **1**$^{2+}$ is wrapped by the naphthalene rings, with the two N^+ atoms of **1**$^{2+}$ equidistant from the methylene mean plane of the host ($^+$N···N$^+$ centroid of **1**$^{2+}$ lies in the CH_2 mean plane of *c*-**PrS[5]^{Me}**). The macroring becomes a nearly regular pentagonal prism upon threading of the 1,4-dihexyl-DABCO **1**$^{2+}$ axle.

In this orientation, the methylene groups of the central DABCO unit of **1**$^{2+}$ establishes eight C–H···π interactions with the four 1,5-bridged naphthalene units (C–H···$\pi^{centroid}$ average distance of 2.5 Å and an average C–H···$\pi^{centroid}$ angle of 143°). The 1,4-bridged naphthalene ring of the complexed host *c*-**PrS[5]^{Me}** adopts a canting angle[30] of 65°, and experiences a large rotation upon threading with **1**$^{2+}$. Significantly, while a very weak C–H···A π interaction with the guest is observed for the 1,4-bridged naphthalene (CH···$\pi^{centroid}$ distance of 2.7 Å and C–H···$\pi^{centroid}$ angle of 108°), its 2-methoxy group establishes a more significant H-bonding interaction with the $^+NCH_2$ group of the DABCO unit of the axle **1**$^{2+}$ with a C–H···O distance of 2.4 Å and a C–H···O angle of 149°.[31] The conformation of the nearly regular pentagonal prism is stabilized by an intramolecular ArC–H···OMe H-bond[31] network formed by the methoxy groups and aromatic H atoms of adjacent naphthalene moieties (Figure 4a, right). In particular, the aromatic hydrogens in positions 4 and 8 (3 and 8 in the 1,4-bridged naphthalene group) are involved in a total of nine intramolecular H-bonds (average H···O distance of 2.1 Å and average C–H···O angle of 150°). The 6-methoxy group of the confused moiety and the adjacent aromatic CH are not part of this regular circular network. It should be noted that two of these stabilizing H-

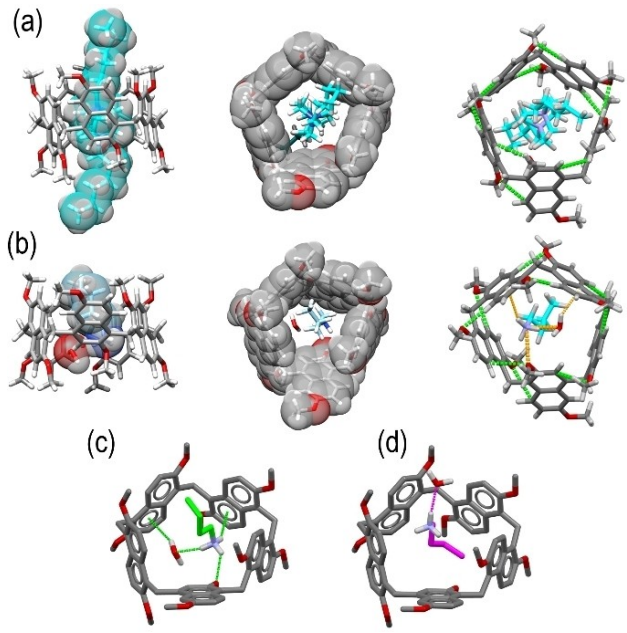

Figure 4. X-ray structural models of the host–guest complexes: a) $\mathbf{1}^{2+}$@(p*R*)$_5$-*c*-**PrS[5]^{Me}**, b) (*U*)-$\mathbf{2}^{+}$@(p*R*)$_5$-*c*-**PrS[5]^{Me}**. Left: side views of the complexes with the guest molecules as vdW spheres. Center: top views of the complexes with the host molecules as vdW spheres. Right: bottom views of the complexes with the stabilizing intramolecular C–H···OMe H-bonds as dashed green lines and the host–guest interactions as dashed orange lines. Top views of the stick representations of the c) *up* (70%) and d) *down* (30%) directional isomers found in the X-ray structure of the $\mathbf{2}^{+}$@*c*-**PrS[5]^{Me}** complex.

bonding interactions would be lost in the heterochiral orientations of the naphthalene flap, in addition to the presence of a destabilizing repulsive interaction between *syn*-oriented OMe groups. In solution, the flipping of the 1,4-bridged naphthalene unit of *c*-**PrS[5]^{Me}** upon threading with $\mathbf{1}^{2+}$ was ascertained by downfield shifts of the resonances attributable to 2-OMe and 3-ArH H-atoms (Figure 3c). In detail, the 2-OMe group is shifted from −0.27 (for the free host in Figure 3a, blue signal) to 3.88 ppm (upon threading of $\mathbf{1}^{2+}$, in Figure 3c), while the 3-ArH atom is downfield shifted from 4.70 to 7.70 ppm (Figure 3cm red signals). These values confirm that the 2-OMe and 3-ArH groups are pushed out from the cavity of *c*-**PrS[5]^{Me}** upon complexation with $\mathbf{1}^{2+}$. In addition, the formation of the $\mathbf{1}^{2+}$@*c*-**PrS[5]^{Me}** pseudorotaxane was ascertained by the presence of ^{1}H NMR signals at negative value of chemical shifts (from −0.8 to −2.0 ppm) attributable to the H atoms of the central bicyclic unit of $\mathbf{1}^{2+}$ threaded inside the macrocycle (Figure 3c). The complexation process between $\mathbf{1}^{2+}$ and *c*-**PrS[5]^{Me}** is slow on the NMR timescale and the ^{1}H NMR signals of the free and complexed *c*-**PrS[5]^{Me}** were identified in Figure 3c.

Finally, the conformational all-p*R* (all-p*S*) homochirality of the host, was confirmed by 1D and 2D NMR analysis. An association constant value of 470 ± 65 M^{-1} was determined for the formation of this pseudorotaxane.[19]

In summary, in the presence of $\mathbf{1}^{2+}$, the *c*-**PrS[5]^{Me}** macrocycle shows a conformationally adaptive behavior and forms a pseudorotaxane structure in which the macrocycle *c*-**PrS[5]^{Me}** adopts a homochiral all-p*R* (all-p*S*) conformation. DFT studies at B97D3/SVP level of theory confirmed that the complex $\mathbf{1}^{2+}$@(p*R*)$_5$-*c*-**PrS[5]^{Me}** is more stable by 2.3 kcal mol^{-1} than the stereoisomer $\mathbf{1}^{2+}$@p*S*(p*R*)$_4$-*c*-**PrS[5]^{Me}** (Supporting Information). Analogously, the threading of the symmetric $\mathbf{3}^{+}$ dibutylammonium cation inside the cavity of the *c*-**PrS[5]^{Me}** host is also stereoselective. 2D NMR investigations (HSQC and COSY) indicated the formation of a single complex. DFT calculations indicated that the homochiral complex $\mathbf{3}^{+}$@(p*R*)$_5$-*c*-**PrS[5]^{Me}** is more stable by 1.5 kcal mol^{-1} than the stereoisomer $\mathbf{3}^{+}$@p*S*-(p*R*)$_4$-*c*-**PrS[5]^{Me}** (Supporting Information, Figure 2b). The flipping of the 1,4-bridged naphthalene unit due to the formation of the $\mathbf{3}^{+}$@(p*R*)$_5$-*c*-**PrS[5]^{Me}** was ascertained by downfield shifts of the resonances attributable to 2-OMe and 3-ArH H atoms of the host (Supporting Information). In detail, the 2-OMe group is shifted from −0.27 to 3.03 ppm, while the 3-ArH group is shifted from 4.70 to 5.60 ppm. DFT calculations show that upon threading with the axle $\mathbf{3}^{+}$, the 1,4-bridged naphthalene ring of *c*-**PrS[5]^{Me}** adopts a canting angle of 42°, which indicates a flipping angle smaller than that experienced by *c*-**PrS[5]^{Me}** upon threading with $\mathbf{1}^{2+}$. DFT-optimized structure of the $\mathbf{3}^{+}$@(p*R*)$_5$-*c*-**PrS[5]^{Me}** complex (Supporting Information) evidenced the presence of a H-bonding interaction between $^{+}NH_2$ group of the axle and the 2-OMe group of the 1,4-bridged naphthalene ring, with a $^{+}$N···O distance of 2.8 Å. An association constant value of 325 ± 40 M^{-1} was calculated for the formation of $\mathbf{3}^{+}$@(p*R*)$_5$-***c*-PrS[5]^{Me}** from ^{1}H NMR data. This value is slightly higher than that reported previously for the formation of the analogous di-*N*-pentyl ammonium complex (190 M^{-1}).[19,20]

With regard to the *endo*-cavity complexation of *c*-**PrS[5]^{Me}** with *n*-butylammonium $\mathbf{2}^{+}$ as barfate salt, X-ray investigation (Figure 4b) confirmed the stereoselective formation of the homochiral $\mathbf{2}^{+}$@*c*-**PrS[5]^{Me}** complex (Figures 4b and 2c). Interestingly, upon *endo*-cavity complexation with $\mathbf{2}^{+}$ the 1,4-bridged ring of the host adopts a canting angle of 38°, significantly lower than the analogous value found in the pseudorotaxane complex $\mathbf{1}^{2+}$@(p*R*)$_5$-*c*-**PrS[5]^{Me}** (Figure 4a). This result clearly indicates that a smaller rotation of the 1,4-bridged flap of the *c*-**PrS[5]^{Me}** host (for p*S*(p*R*)$_4$ enantiomer) is required to allow *endo*-cavity complexation of $\mathbf{2}^{+}$, with respect to the threading process with $\mathbf{1}^{2+}$. The above-described characteristic intramolecular C_{Ar}H···OMe H-bond network involving adjacent naphthalene groups is also observed for this complex (Figure 4b, right). However, while the interactions between the 1,5-naphthalene groups are similar (six H-bonds with an average distance of 2.1 Å and an average angle of 167°), the H-bond interactions involving the 1,4-linked naphthalene show a much less significant direction characteristic due to the smaller flap rotation (three very weak interactions with an average distance of 2.8 Å and average angle of 99°). The butyl ammonium guest is inserted in the macrocycle so that the charged head forms three strong H-bonds (Figure 4c): i) with the 2-OMe group of the flap (H···O distance of 2.1 Å and N–H···O angle of 132°); ii) with an aromatic ring of a 1,5-linked naphthalene (H···$\pi^{centroid}$ distance of 2.7 Å and N–H···$\pi^{centroid}$ angle of 151°); and iii) with a hosted water molecule (H···O distance of 1.9 Å and N–H···O

angle of 164°). This hosted water molecule also forms a synergic OH···π hydrogen bond (Figure 4c) with an aromatic ring (H···$\pi^{centroid}$ distance of 2.4 Å and O–H···$\pi^{centroid}$ angle of 145°).

It is interesting to note that the directional stereochemistry of the racemic complex is predominantly *up* (*U*)-**2**$^{+}$@(p*R*)$_5$-*c*-**PrS[5]**^{Me} and (*U*)-**2**$^{+}$@(p*S*)$_5$-*c*-**PrS[5]**^{Me} (Figures 4c, d and 5a). However, the X-ray structure shows, together with thelower occupancy factor (0.3), the inverted orientation of the **2**$^{+}$ directional guest corresponding to the *down* steroisomeric complexes (*D*)-**2**$^{+}$@(p*R*)$_5$-*c*-**PrS[5]**^{Me} and (*D*)-**2**$^{+}$@(p*S*)$_5$-*c*-**PrS[5]**^{Me} (Figures 4d and 5e, f, see the Supporting Information). In this case, the stabilizing host-guest ammonium interactions are largely absent. When **2**$^{+}$ as barfate salt was added to a CD_2Cl_2 solution of *c*-**PrS[5]**^{Me}, the ^{1}H NMR spectrum in Figure 3b, of the mixture (equimolar) shows a typical signature at high-field negative values characteristic of an *endo*-complexation of the butyl chains of **2**$^{+}$ shielded by naphthalene rings (0.60, −0.55, −0.21, and 0.09 ppm for α, β, γ, and δ, respectively; Figure 3b, green signals).

2D COSY, HSQC, and NOESY experiments clearly show the selective formation in solution of (*U*)-**2**$^{+}$@(p*R*)$_5$-*c*-**PrS[5]**^{Me}. In fact, diagnostic dipolar couplings (Figure S31 in the Supporting Information) are present between H(α) (0.60 ppm) of **2**$^{+}$ and 3-ArH (5.34 ppm) of *c*-**PrS[5]**^{Me} host (Figure 5e).

The DFT-optimized structure of the (*U*)-**2**$^{+}$@(p*R*)$_5$-*c*-**PrS[5]**^{Me} complex shows the presence of stabilizing H-bonding interactions between $^{+}NH_3$ group of **2**$^{+}$ and 2-OMe group of *c*-**PrS[5]**^{Me}. An association constant value of 1000 ± 160 M^{-1} was evaluated by ^{1}H NMR analysis. With these results in hand, the directional threading of *c*-**PrS[5]**^{Me} with cations **4**$^{2+}$ and **5**$^{2+}$ was investigated (Figures 2c and 5). In this case four stereoisomeric *up/down* complexes can be potentially formed.[28a] The addition of 1-hexyl-4-isopropyl-DABCO **4**$^{2+}$ as barfate salt to *c*-**PrS[5]**^{Me} in CD_2Cl_2 clearly evidences the formation of a pseudorotaxane complex in which the macrocycle adopts a homochiral all-p*R* conformation. 2D NOESY experiment evidences the stereoselective formation of the *down* stereoisomer (*D*)-**4**$^{2+}$@(p*R*)$_5$-*c*-**PrS[5]**^{Me} (Figure 5). In fact diagnostic dipolar couplings (Supporting Information) are present in the NOESY spectrum of the pseudo[2]rotaxane, between H5 (−0.73 ppm) of *down*-oriented **4**$^{2+}$ and 3-ArH atom (7.70 ppm) of *c*-**PrS[5]**^{Me} host (Figures 5c) and between and H7 atoms (−0.58 ppm) of **4**$^{2+}$ and 3-ArH atom of *c*-**PrS[5]**^{Me}. DFT calculations indicate that the complex (*D*)-**4**$^{2+}$@(p*R*)$_5$-*c*-**PrS[5]**^{Me} is more stable by 2.5 kcal mol^{-1} than the *U*-stereoisomer. Closer inspection of the DFT-calculated structures of *up* and *down* **4**$^{2+}$@(p*R*)$_5$-*c*-**PrS[5]**^{Me} pseudorotaxanes reveals that the *down*-oriented **4**$^{2+}$ axle penetrates more deeply into the cavity of *c*-**PrS[5]**^{Me} (Supporting Information). In fact, the $^{+}$N···N^{+} centroid of the central DABCO unit of the axle is sitting at 0.8 Å above the mean plane of the methylene groups of the host, a value significantly lower with respect to that measured for the *up*-stereoisomer (1.2 Å). Thus, in the *down*-orientation, the central DABCO unit establishes a larger contact area with the cavity of the prismarene, and 10 C–H···π interactions (mean CH···$\pi^{centroid}$ distance of 2.6 Å (Supporting Information)) are observed. Differently, the DFT-optimized structure of the stereoisomeric *(U)*-**4**$^{2+}$@(p*R*)$_5$-*c*-**PrS[5]**^{Me} shows only 4 C–H···π interactions with a mean C–H···$\pi^{centroid}$ distance of 2.6 Å (Supporting Information).

1D and 2D NMR analysis of an equimolar mixture of **5**$^{2+}$ and *c*-**PrS[5]**^{Me} (Figure 3d) indicates the formation of the *(D)*-**5**$^{2+}$@(p*R*)$_5$-*c*-**PrS[5]**^{Me} pseudorotaxane. Analogously, the *down*-orientation (Figure 5) was ascertained by 2D NOESY experiment (Figure S22). A diagnostic dipolar coupling (Supporting Information) is present between $N^{+}CH_3$ (2.02 ppm) group of **5**$^{2+}$ and 2-OMe (3.94 ppm) of *c*-**PrS[5]**^{Me} host (Figure 5d). In addition, a diagnostic cross-peak is present in the NOESY spectrum of the complex between 2-OMe (3.94 ppm) of *c*-**PrS[5]**^{Me} host and CH_2(2) atoms of the axle **5**$^{2+}$ (0.94 and 0.74 ppm, Figure S22). These results evidenced the stereoselective formation of the *down*-stereoisomer (*D*)-**5**$^{2+}$@(p*R*)$_5$-*c*-**PrS[5]**^{Me} (Figure 5), and DFT results confirm the larger stability of the *down*-stereoisomer with respect to *up* (△*E* = 3.6 kcal mol^{-1}). Analysis of the DFT-optimized structures of the *up* and *down* **5**$^{2+}$@(p*R*)$_5$-*c*-**PrS[5]**^{Me} stereoisomers, reveals that in the *down* orientation, the centroid ($^{+}$N···N^{+}) of the DABCO unit of **5**$^{2+}$ is at a distance of 0.31 Å from the CH_2-mean plane of *c*-**PrS[5]**^{Me}, significantly lower than that measured in the *up* orientation of **5**$^{2+}$ (1.62 Å). Also in this case, the deeper penetration of the DABCO unit inside the cavity of the macrocycle of the (*D*)-**4**$^{2+}$@(p*R*)$_5$-*c*-**PrS[5]**^{Me} complex ensures larger contact area between host and guest to give more favorable C–H···π interactions (Supporting Information). NMR spectra showed that a higher binding affinity is achieved for the complexation of 1-hexyl-4-isopropyl-DABCO **4**$^{2+}$ with respect to 1-hexyl-4-methyl-DABCO **5**$^{2+}$, with *K* values of 800 ± 130 and 500 ± 70 M^{-1}, respectively.

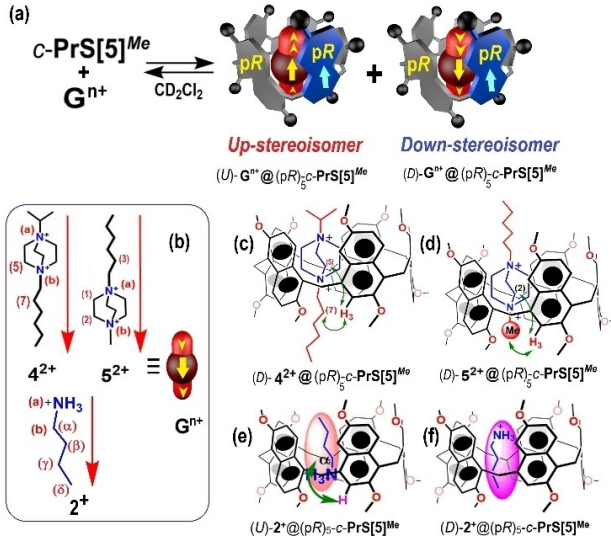

Figure 5. a) Schematic representation of the threading equilibrium between *c*-**PrS[5]**^{Me} host and directional ammonium guests **2**$^{+}$, **4**$^{2+}$, and **5**$^{2+}$. b) For the assignment of *up* and *down* directionality of the axles, see ref. [28a]. c)–f) Chemical drawings of the *up*/*down* stereoisomers. Green arrows highlight the diagnostic dipolar couplings observed in the NOESY spectra (Supporting Information).

Conclusions

The confused-prism[5]arene macrocycle shows conformationally adaptive behavior in the presence of appropriate ammonium guests. After the inclusion processes, a homochiral conformation of the host was observed that inverts the planar chirality of the 1,4-naphtalene flap (from p*S* to p*R* and vice versa). X-ray studies supported by DFT calculations demonstrate that the homochiral all-p*R* (all-p*S*) complexes are stabilized by favorable intramolecular and intermolecular C–H···π interactions.

A stereoselective directional threading is also observed in the presence of directional axles; these *up* and *down* directional isomers double the possible number of stereoisomers. In fact, in the case of the primary alkylammonium $\mathbf{2}^{+}$ a preference for the *up* stereoisomer is observed in the solid state and in solution (Figures 4 and 5), whereas $\mathbf{4}^{2+}$ and $\mathbf{5}^{2+}$, assume a down orientation in solution (Figure 5). Therefore, the symmetry breaking introduced by the 1,4-link in confused-prismarenes creates a new scenario in terms of the stereochemistry of these systems, characterized by a conformationally adaptive macrocycle that can easily open the 1,4-bridged naphthalene flap in a stereoselective manner.

Experimental Section

General: HR MALDI mass spectra were recorded on a Bruker Solaris XR Fourier transform ion cyclotron resonance mass spectrometer equipped with a 7T refrigerated actively shielded superconducting magnet. All samples were recorded in MALDI (8 laser shots were used for each scan) and they were prepared by mixing 10 μL of analyte in dichloromethane or methanol (1 mg mL^{-1}) with 10 μL of solution of 2,5-dihydroxybenzoic acid (10 mg mL^{-1} in MeOH). The mass spectra were calibrated externally, and a linear calibration was applied. All chemical reagents grade was used without further purification and were used as purchased by TCI and Merck. Reaction temperatures were measured externally. Reactions were monitored by Merck TLC silica gel plates (0.25 mm) and visualized by UV light 254 nm, or by spraying with H_2SO_4-$Ce(SO_4)_2$. NMR spectra were recorded on a Bruker Avance-600 [600 (^{1}H) and 150 MHz (^{13}C)] and Avance-300 [300 (^{1}H) and 75 MHz (^{13}C)] spectrometers. Chemical shifts are reported relative to the residual solvent peak.[32] Standard pulse programs, provided by the manufacturer, were used for 2D COSY (cosygpqf), 2D HSQC (hsqcedetgpsisp2.2) and 2D NOESY (noesygpphpp) experiments. Structural assignments were made with additional information from gCOSY, gHSQC, and geNOESY experiments. Derivative *c*-**PrS[5]^{Me}** was synthesized as reported.[19]

Deposition Numbers 2070351 (for $\mathbf{1}^{2+}$@*c*-PrS[5]^{Me}) and 2070352 (for $\mathbf{2}^{+}$@*c*-PrS[5]^{Me}) contain the supplementary crystallographic data for this paper. These data are provided free of charge by the joint Cambridge Crystallographic Data Centre and Fachinformationszentrum KarlsruheAccess Structures service.

Synthesis of $\mathbf{4}\cdot(\mathbf{BArF})_2$: A solution of 1-hexyl-4-aza-1-azoniabicyclo[2.2.2]octane Iodide[33] (0.28 g, 0.87 mmol) in acetonitrile (25 mL) was stirred for 10 min. Subsequently, isopropyl iodide (0.59 g, 3.51 mmol) was added, and the mixture was stirred at room temperature for 16 h. A precipitate was formed which was filtered, washed several times with petroleum ether (3×10 mL), and dried under reduced pressure at 80 °C to give 1-hexyl-4-isopropyl-1,4-diazabicyclo[2.2.2]octane-1,4-diium iodide as intermediate. The bis-iodide derivative was dissolved in methanol (25 ml) and NaBArF was added (1.55 g, 1.75 mmol), and the mixture was stirred at room temperature for 16 h. The solvent was removed under reduced pressure and subsequently the residue was washed several times with H_2O (3×10 mL) to give derivative $\mathbf{4}\cdot(BArF)_2$ as a light brown powder (1.54 g, 90%). ^{1}H NMR (300 MHz, CD_3OD, 298 K): $\delta = 7.59$ (overlapped, ArH, 24H), 3.96-3.90 (overlapped, NC*H*$(CH_3)_2$, NCH_2, 13H), 3.54 (m, NCH_2, 2H), 1.83 (m, CH_2, 2H), 1.51-1.38 (overlapped, CH(CH_3)$_2$, CH_2, 12H), 0.94 (t, CH_3, $J = 7.0$ Hz, 3H). ^{13}C NMR {^{1}H} (150 MHz, CD_2Cl_2, 298 K): $\delta = 162.6$, 162.3, 162.0, 161.6, 135.2, 129.5, 129.3, 129.1, 128.9, 127.7, 125.9, 124.1, 122.3, 118.0, 71.9, 67.9, 52.1, 49.1, 31.2, 25.6, 22.9, 22.5, 16.7, 13.7. HRMS (MALDI): *m/z* calcd for $C_{47}H_{44}BF_{24}N_2^+$: 1103.3209 [*M*-BArF$^-$]$^+$; found 1103.3183.

Synthesis of $\mathbf{5}\cdot(\mathbf{BArF})_2$: A solution of 1-hexyl-4-aza-1-azoniabicyclo[2.2.2]octane iodide[33] (0.28 g, 0.87 mmol) in acetonitrile (25 mL) was stirred for 10 min. Subsequently, methyl iodide (0.50 g, 3.51 mmol) was added, and the mixture was stirred at room temperature for 16 h. The thus formed precipitate was filtered, washed several times with petroleum ether (3×10 mL), and dried under reduce pressure at 80 °C to give 1-hexyl-4-methyl-1,4-diazabicyclo[2.2.2]octane-1,4-diium iodide as intermediate. The bis-iodide derivative was dissolved in methanol (25 mL) and NaBArF was added (1.55 g, 1.75 mmol), and the mixture was stirred at room temperature for 16 h. The solvent was removed under reduced pressure, and subsequently the residue was washed several times with H_2O (3×10 mL) to give derivative $\mathbf{5}\cdot(BArF)_2$ as a light brown powder (1.58 g, 95%). ^{1}H NMR (600 MHz, CD_2Cl_2, 298 K): $\delta = 7.73$ (s, ArH, 16H), 7.59 (s, ArH, 8H), 4.00–3.90 (overlapped, NCH_2, 12H), 3.54 (m, NCH_2, 2H), 3.48 (s, NCH_3, 3H), 1.80 (m, CH_2, 2H), 1.46-1.32 (overlapped, CH_2, 6H), 0.90 (t, CH_3, $J = 7.0$ Hz, 3H). ^{13}C NMR {^{1}H} (150 MHz, CD_2Cl_2, 298 K): $\delta = 162.6$, 162.3, 162.0, 161.6, 135.2, 129.5, 129.3, 129.1, 128.9, 127.8, 126.0, 124.1, 122.3, 118.0, 68.3, 54.9, 54.5, 52.0, 31.2, 25.6, 22.9, 22.5, 13.7. HRMS (MALDI): *m/z* calcd for $C_{45}H_{40}BF_{24}N_2^+$ 1075.2896 [*M*-BArF$^-$]$^+$; found 1075.2887.

^{1}H NMR determination of K_{ass} values: The association constant values for the formation of the complexes were calculated by two methods:

a) Integration of ^{1}H NMR signals of free and complexed host. In this case, an equimolar solution of hosts and guests was solubilized in CD_2Cl_2, and analyzed immediately after mixing.
b) ^{1}H NMR competition experiments. In this case, an analysis of a 1:1:1 mixture of host, and two guests in an NMR tube with CD_2Cl_2 as solvent was performed immediately after mixing.

All K_{ass} values were calculated at 183 K, and ^{1}H NMR experiments were recoded on a 600 MHz spectrometer. Errors $< 15\%$ were calculated as mean values of three measures.

Computational details: The B97D3 functional was adopted for all DFTcomputations.[34] The density fitting approximation was employed for the Coulomb problem; the proper auxiliary basis set by Weigend was used throughout.[35] Solvent (dichloromethane) effects were included in all DFT computations according to the polarizable continuum model.[36] MM computations carried out before the conformer search were performed by using the Spartan software.[37] The Gaussian package was employed for DFT computations.[38] The TZVP basis set was used in DFT optimizations of the conformers, whereas the SVP basis set was adopted for the geometry optimizations of binary complexes. The starting structures of binary complexes were obtained by MM calculations performed by using the YASARA software.

Crystallographic structures of $\mathbf{1}^{2+}$@ *c*-PrS[5]^{Me} and $\mathbf{2}^{+}$@ *c*-PrS[5]^{Me}: Single crystals suitable for X-ray investigation were obtained by slow evaporation of CH_2Cl_2/hexane solutions containing 1,4-confused prism[5]arene ***c*-PrS[5]^{Me}** in the presence of barfate ($BArF^-$)

salts of *N,N'*-dihexyl-1,4-diazabicyclo[2.2.2]octane ($\mathbf{1}^{2+}$) or *n*-butylammonium ($\mathbf{2}^{+}$). Data collection was conducted at the XRD1 beamline of the Elettra synchrotron (Trieste, Italy), employing the rotating-crystal method with a Dectris Pilatus 2 M area detector. The single crystals investigated were dipped in a cryo-protectant (Paratone), mounted on a nylon loop and flash-frozen under a nitrogen stream at 100 K. Diffraction data were indexed and integrated using the XDS package,[39] while scaling was carried out with XSCALE.[40] The structures were solved using the SHELXT program[41] and structure refinement was performed with SHELXL-2018/3,[42] operating through the WinGX GUI,[43] by full-matrix least-squares (FMLS) methods on F^2. The thermal parameters of all non-hydrogen atoms were refined anisotropically, except for atoms below 50% occupancy. Hydrogen atoms were placed at the calculated positions and refined using the riding model. Crystallographic data (and final refinement details for the structures) are reported in Table S3.

Conflict of Interest

The authors declare no conflict of interest.

Data Availability Statement

The data that support the findings of this study are available in the supplementary material of this article.

Keywords: directional · molecular recognition · prismarenes · pseudorotaxanes · stereoselectivity

[1] F. Diederich, P. J. Stang, R. R. Tykwinski in *Modern Supramolecular Chemistry: Strategies for Macrocycle Synthesis*; Wiley-VCH, Weinheim, **2008**.

[2] P. Della Sala, C. Talotta, A. Capobianco, A. Soriente, M. De Rosa, P. Neri, C. Gaeta, *Org. Lett.* **2018**, *20*, 7415–7418.

[3] S. Gambaro, C. Talotta, P. Della Sala, A. Soriente, M. De Rosa, C. Gaeta, P. Neri, *J. Am. Chem. Soc.* **2020**, *142*, 14914–14923.

[4] M. Raynal, P. Ballester, A. Vidal-Ferran, P. W. N. M. van Leeuwen, *Chem. Soc. Rev.* **2014**, *43*, 1660–1733.

[5] *Calixarenes and Beyond* (Eds.: P. Neri, J. L. Sessler, M.-X. Wang), Springer, Dordrecht, **2016**

[6] D. J. Cram, J. M. Cram, *Container Molecules and Their Guests*, Royal Society of Chemistry, Cambridge, **1997**.

[7] *Pillararenes* (Ed.: T. Ogoshi), Royal Society of Chemistry, Cambridge, **2015**.

[8] H. Yao, W. Jiang in *Handbook of Macrocyclic Supramolecular Assembly* (Eds.: Y. Liu, Y. Chen, H.-Y. Zhang), Springer, Singapore, **2020**, pp. 975–995.

[9] L.-P. Yang, X. Wang, H. Yao, W. Jiang, *Acc. Chem. Res.* **2020**, *53*, 198–208.

[10] R. Del Regno, P. Della Sala, A. Spinella, C. Talotta, D. Iannone, S. Geremia, N. Hickey, P. Neri, C. Gaeta, *Org. Lett.* **2020**, *22*, 6166–6170.

[11] F. Jia, Z. He, L.-P. Yang, Z.-S. Pan, M. Yi, R.-W. Jiang, W. Jiang, *Chem. Sci.* **2015**, *6*, 6731–6738.

[12] J. Li, H. Zhou, Y. Han, C. Chen, *Angew. Chem. Int. Ed.* **2021**, *60*, 21927–21933.

[13] X. Wang, J. Jia, L.-P. W. Yang, H. Zhou, W. Jiang, *Chem. Soc. Rev.* **2020**, *49*, 4176–4188. F. Jia, D.-H. Li, S. He, L.-P. Yang, W. Jiang, *Angew. Chem. Int. Ed.* **2022**, e202212305.

[14] a) G. G. Hammes, Y.-C. Chang, T. G. Oas, Proc . *Natl. Acad. Sci. USA* **2009**, *106*, 13737–13741; b) J. Monod, J. Wyman, J.-P. Changeux, *J. Mol. Biol.* **1965**, *12*, 88–188.

[15] F. Paul, T. R. Weikl, *PLoS Comput. Biol.* **2016**, 1–17.

[16] D. E. Koshland, *Proc. Nat. Acad. Sci.* USA **1958**, *44*, 98–104.

[17] Very recently, it has been show that topoisomerases I (TOP1) of eukaryotes, which are widely distributed enzymes removing DNA torsional stress, display a transition from an open to a closed conformation upon DNA binding. The authors report that the change in conformation is caused by rotation between the capping (CAP) and the catalytic (CAT) domains.D. T. Takahashi, D. Gadelle, K. Agama, E. Kiselev, H. Zhang, E. Yab, S. Petrella, P. Forterre, Y. Pommier, C. Mayer, *Nat. Commun.* **2022**, *13*, doi.org/10.1038/s41467-021-27686-7.

[18] M. De Rosa, C. Talotta, C. Gaeta, A. Soriente, P. Neri, S. Pappalardo, G. Gattuso, A. Notti, M. F. Parisi, I. Pisagatti, *J. Org. Chem.* **2017**, *82*, 5162–5168.

[19] P. Della Sala, R. Del Regno, C. Talotta, A. Capobianco, N. Hickey, S. Geremia, M. De Rosa, A. Spinella, A. Soriente, P. Neri, C. Gaeta, *J. Am. Chem. Soc.* **2020**, *142*, 1752–1756.

[20] P. Della Sala, R. Del Regno, L. Di Marino, C. Calabrese, C. Palo, C. Talotta, S. Geremia, N. Hickey, A. Capobianco, P. Neri, C. Gaeta, *Chem. Sci.* **2021**, *12*, 9952–9961.

[21] R. Del Regno, P. Della Sala, D. Picariello, C. Talotta, A. Spinella, P. Neri, C. Gaeta, *Org. Lett.* **2021**, *23*, 8143–8146.

[22] R. Del Regno, G. D. G. Santonoceta, P. Della Sala, M. De Rosa, A. Soriente, C. Talotta, A. Spinella, P. Neri, C. Sgarlata, C. Gaeta, *Org. Lett.* **2022**, *24*, 2711–2715.

[23] L.-P. Yang, W. Jiang, *Angew. Chem. Int. Ed.* **2020**, *7*, 15794–15796.

[24] Z. Canja, I. Lyle, *Chem. Eur. J.* **2022**, *28*, e202201743.

[25] Very recently, an analogous template effect was observed for the synthesis of methylene-bridged naphthotubes: Y.-F. Wang, H. Yao, L.-P. Yang, M. Quan, W. Jiang *Angew. Chem. Int. Ed.* **2022**, *61*, e202211853.

[26] T. Ogoshi, K. Masaki, R. Shiga, K. Kitajima, T. Yamagishi, *Org. Lett.* **2011**, *13*, 1264–1266.

[27] Previously, it has been shown that the conformation of cyclophane macrocycles can be described by the signs of $ArCH_2Ar$ torsional angles: G. Bifulco, L. Gomez-Paloma, R. Riccio, C. Gaeta, F. Troisi, P. Neri, *Org. Lett.* **2005**, *7*, 5757–5760.

[28] a) The directionality of axles such as $\mathbf{2}^{+}$, $\mathbf{4}^{2+}$, and $\mathbf{5}^{2+}$, is assigned by an arrow whose orientation is determined as follows: using the CIP rules, determine the atom "A" of highest priority of the axle and the next priority atom "B" that allow the axle direction to be assigned from "A" to "B" (Figure 5 < xfigr5; b). The *up* or *down* orientation of axles is determined with respect to the 2-OMe group of the confused naphthalene moiety, which defines the lower side of the macroring (Figure 5a, and 2c); b) For a review on the chirality in interpenetrated architectures, see: E. M. G. Jamieson, F. Modicom, S. M. Goldup, *Chem. Soc. Rev.* **2018**, *47*, 5266–5311.

[29] BArF anion = (tetrakis[3,5-bis(trifluoromethyl)phenyl]borate), has been widely used in molecular recognition processes with ammonium guests: C. Gaeta, F. Troisi, P. Neri, *Org. Lett.* **2010**, *12*, 2092–2095.

[30] The canting angle is defined as the dihedral angle between the naphthalene plane and the mean plane of the bridging methylene carbon atoms of the prism[*n*]arene molecule.

[31] T. Steiner, *Angew. Chem. Int. Ed.* **2002**, *41*, 48–76; *Angew. Chem.* **2002**, *114*, 50–80.

[32] G. R. Fulmer, A. J. M. Miller, N. H. Sherden, H. E. Gottlieb, A. Nudelman, B. M. Stoltz, J. E. Bercaw, K. I. Goldberg, *Organometallics* **2010**, *29*, 2176–2179.

[33] J.-Y. Kazock, M. Taggougui, B. Carré, P. Willmann, D. Lemordant, *Synthesis* **2007**, *2007*, 3776–3778.

[34] a) T. Schwabe, S. Grimme, *Phys. Chem. Chem. Phys.* **2006**, *8*, 4398–4401; b) P. Della Sala, A. Capobianco, T. Caruso, C. Talotta, M. De Rosa, P. Neri, A. Peluso, C. Gaeta, *J. Org. Chem.* **2018**, *83*, 220–227.

[35] a) F. Weigend, *Phys. Chem. Chem. Phys.* **2006**, *8*, 1057–1065; b) B. I. Dunlap, *J. Mol. Struct.* **2000**, *529*, 37–40.

[36] J. Tomasi, B. Mennucci, R. Cammi, *Chem. Rev.* **2005**, *105*, 2999–3094.

[37] Spartan'04, Wavefunction, Inc., Irvine, CA.

[38] *Gaussian 16, Revision C.01*, M. J. Frisch, G. W. Trucks, H. B. Schlegel, G. E. Scuseria, M. A. Robb, J. R. Cheeseman, G. Scalmani, V. Barone, G. A. Petersson, H. Nakatsuji, X. Li, M. Caricato, A. V. Marenich, J. Bloino, B. G. Janesko, R. Gomperts, B. Mennucci, H. P. Hratchian, J. V. Ortiz, A. F. Izmaylov, J. L. Sonnenberg, D. Williams-Young, F. Ding, F. Lipparini, F. Egidi, J. Goings, B. Peng, A. Petrone, T. Henderson, D. Ranasinghe, V. G. Zakrzewski, J. Gao, N. Rega, G. Zheng, W. Liang, M. Hada, M. Ehara, K. Toyota, R. Fukuda, J. Hasegawa, M. Ishida, T. Nakajima, Y. Honda, O. Kitao, H. Nakai, T. Vreven, K. Throssell, J. A. Montgomery, Jr., J. E. Peralta, F. Ogliaro, M. J. Bearpark, J. J. Heyd, E. N. Brothers, K. N. Kudin, V. N. Staroverov, T. A. Keith, R. Kobayashi, J. Normand, K. Raghavachari, A. P. Rendell, J. C. Burant, S. S. Iyengar, J. Tomasi, M. Cossi, J. M. Millam, M.

Klene, C. Adamo, R. Cammi, J. W. Ochterski, R. L. Martin, K. Morokuma, O. Farkas, J. B. Foresman, D. J. Fox, Gaussian, Inc., Wallingford CT, **2016**.
[39] W. Kabsch, *Acta Crystallogr. Sect. D Biol. Crystallogr.* **2010**, *66*, 125–132.
[40] W. Kabsch, *Acta Crystallogr. Sect. D Biol. Crystallogr.* **2010**, *66*, 133–144.
[41] G. M. Sheldrick, *Acta Crystallogr. Sect. A Found. Adv.* **2015**, *71*, 3–8.
[42] G. M. Sheldrick, *Acta Crystallogr. Sect. A Found. Crystallogr.* **2008**, *64*, 112–122.
[43] L. J. Farrugia, *J. Appl. Crystallogr.* **2012**, *45*, 849–854.

Manuscript received: September 28, 2022
Accepted manuscript online: November 1, 2022
Version of record online: December 5, 2022